Coherent spectroscopy of degenerate two-level systems in Cs

C. Andreeva, S. Cartaleva, and Y. Dancheva
Institute of Electronics, BAS, Boul. Tsarigradsko Shosse 72, 1784 Sofia, Bulgaria

V. Biancalana, A. Burchianti, C. Marinelli, E. Mariotti, and L. Moi*
INFM UdR Siena, Department of Physics, University of Siena, Via Banchi di Sotto 55, 53100 Siena, Italy

K. Nasyrov
Institute of Automation and Electrometry, Novosibirsk, Russia
(Received 5 November 2001; published 11 July 2002)

Coherent spectroscopy of degenerate two-level systems of the Doppler-broadened D_2 cesium line has been performed in vacuum and in buffer gas cells. Subnatural-width (SNW) electromagnetically induced transparency and electromagnetically induced absorption (EIA) resonances have been observed with single-frequency laser excitation for different light polarizations and collision regimes. SNW-EIA resonances with linearly polarized excitation of the $F_g=4$ level are observed, and they increase their contrast with power density increase and reach a contrast of 20% at 200 $\mathrm{mW\,cm^{-2}}$. A theoretical model has been elaborated, taking into account the Doppler broadening of the transitions, the linewidth of the laser light, and the experimental conditions for observation of the fluorescence. Here the theoretical results are in agreement with those of the experiment. In a buffer gas cell, the SNW resonances in the fluorescence, in degenerate two-level systems are observed for the first time and they are only obtained with circularly polarized light. A theoretical explanation of this result is proposed. At the expense of contrast, in the presence of a buffer gas the coherent resonances are significantly narrower than in a vacuum cell for the same power density. The observation of SNW resonances in buffer gas is significantly less sensitive to the laser frequency drift than in a vacuum cell, which could be advantageous for applications in metrology and in the measurement of weak magnetic fields.

DOI: 10.1103/PhysRevA.66.012502 PACS number(s): 32.70.Jz, 42.50.Md, 42.50.Gy

I. INTRODUCTION

Interesting coherent effects have been observed in three-level configurations and have attracted considerable attention in recent years. The phenomenon of coherent population trapping (CPT) [1,2] and the related effect of electromagnetically induced transparency (EIT) [3] in Λ systems are among the most important. These effects have found interesting applications in subrecoil laser cooling [4], magnetometry [5], steep dispersion [6], coherent population transfer among atomic and molecular quantum states [7], and ultralow group velocity propagation [8].

Degenerate two-level systems provide further possibilities for the analysis of coherent effects in the interaction of light fields with an atomic sample. It has been shown that these systems are suitable for observation of coherent effects predicted and observed in three-level configurations [9,10]. In addition, they make possible the detection of new effects such as electromagnetically induced absorption (EIA) [11], that have not been observed in three-level configurations.

Optical pumping and nonabsorbing state formation in the case of different degenerate two-level systems irradiated by elliptically polarized laser light are theoretically considered in Ref. [12].

It should be pointed out that coherent effects occurring in degenerate two-level systems have also found a number of applications in practical and fundamental research. Using paraffin coated Rb cell long-lived ground state coherence has been obtained which provides observation of features with relaxation rate $\gamma_{rel}\simeq 2\pi\times 1$ Hz in the nonlinear magneto-optic effect [13]. It has been shown that this technique can be used for weak magnetic field measurements with a remarkable sensitivity of 3×10^{-12} $\mathrm{G}/\sqrt{\mathrm{Hz}}$ [14].

Subnatural-width (SNW) dips and peaks in the fluorescence of rubidium vapor have been studied experimentally and theoretically by excitation of a single hyperfine (hf) transition of the D_2 line by a coherent bichromatic laser field. These resonances have been studied as a function of the frequency difference between the two electromagnetic fields [11,15,16]. Similar coherent resonances have also been observed by using a single-frequency linearly polarized laser excitation [17]. In the last case the Rb fluorescence was measured as a function of the magnetic field intensity, which is modulated around zero value and kept parallel to the laser beam. SNW-EIT or SNW-EIA resonances are observed depending on whether $F_g\rightarrow F_e=F_g$, F_g-1 or $F_g\rightarrow F_e=F_g+1$ hf transitions are excited, as illustrated in Fig. 1. There, F_g and F_e are the quantum numbers representing the total angular momenta of the ground and the excited states, respectively. In the case of a $F_g\rightarrow F_e=F_g-1$ transition [Fig. 1(a)], Λ links are established, which lead to observed dark states (EIT), while in the case of a $F_g\rightarrow F_e=F_g+1$ transition [Fig. 1(b)], V links are formed, which give bright states (EIA). For Λ-link chains, atoms are trapped in a nonabsorbing state, which is a superposition of ground-state Zeeman sublevels, resulting in a strong decrease in the fluorescence [9]. As recently shown [18], for V-link chains, many atoms

*Electronic address: moi@unisi.it

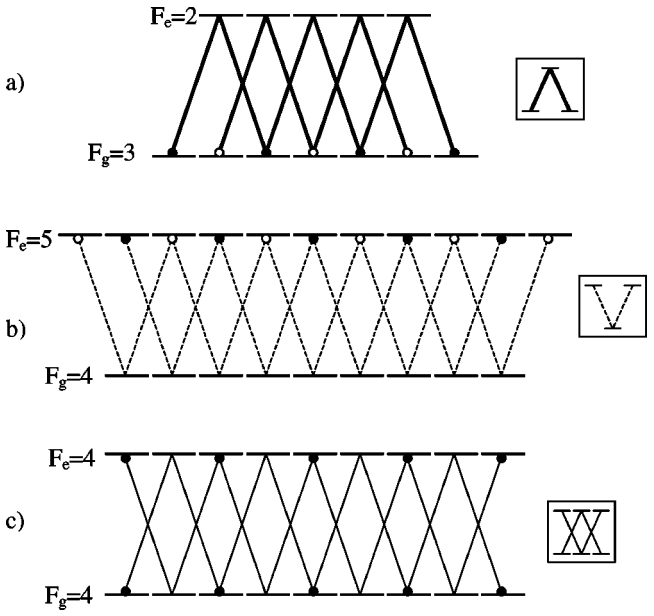

FIG. 1. Illustration of the Λ and V links formation for (a) $F_g \rightarrow F_e = F_g - 1$, (b) $F_g \rightarrow F_e = F_g + 1$, and (c) $F_g \rightarrow F_e = F_g$ transitions.

are accumulated on the ground state levels which have the strongest coupling to the excited state, thus leading to an increase in the fluorescence at zero magnetic field. For $F_g \rightarrow F_e = F_g$ transitions [Fig. 1(c)], although Λ and V links exist, in agreement with the theoretical considerations of [9], only dark states are observed.

In this work we present experimental and theoretical analysis of SNW resonances in Cs vapor. Compared to rubidium, cesium makes possible a simpler and more accurate interpretation of the experimental data due to the absence of other stable isotopes and to the larger separation of the hf levels. The latter makes the overlapping of the corresponding transitions less important leading to better clarification of their relative contribution to the coherent resonances.

We demonstrate that in a Cs cell without buffer gas, the sign of the SNW resonances is determined by the two closed $F_g = 3 \rightarrow F_e = 2$ and $F_g = 4 \rightarrow F_e = 5$ transitions. For laser power densities below the saturation power, at the $F_g = 4 \rightarrow F_e = 5$ transition, the experimental results confirm the recently developed theory [18] (which considers monochromatic laser radiation and homogeneously broadened hf transitions), while for high laser power densities the experimental results are in disagreement with it.

Until now the SNW resonances in the fluorescence or transmitted light for degenerate two-level systems were studied either in atomic beams or in vacuum cells. To our knowledge our report is the first experimental observation of these resonances in the presence of a buffer gas. Using a buffer gas cell, we observe SNW resonances only in the case of circularly polarized excitation.

The experimental results presented here are described by our theoretical model, based on the optical Bloch equations (OBE) solution. In the case of vacuum cell, the Doppler broadening of the hf transition and the effective linewidth of the laser light are taken into account. Unlike the treatment in [18], where the total fluorescence is considered, in our model the fluorescence along different directions is calculated and a direct comparison with the experimental conditions is made possible. For the buffer gas cell, the redistribution of the atoms among the Zeeman sublevels of the excited state due to collisions of the Cs with the buffer gas atoms is also taken into account.

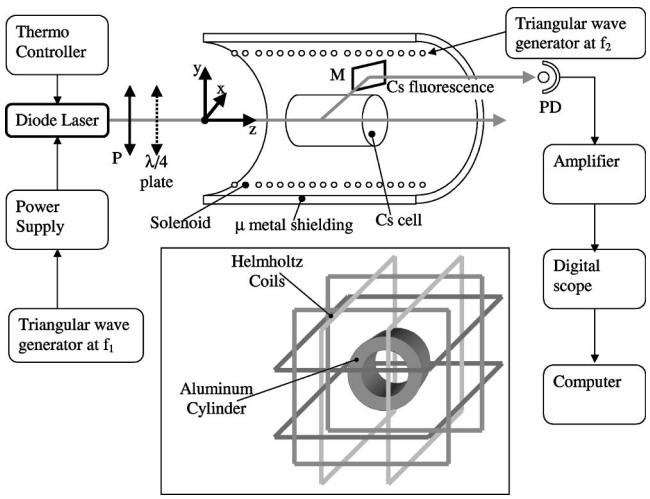

FIG. 2. Experimental setup.

In order to examine the contribution of the different hf transitions to the SNW resonances formation, the contrast of the latter over the fluorescence profiles is measured.

II. EXPERIMENTAL SETUP

The detection of the SNW resonances as a function of the laser frequency position within the Doppler broadened fluorescence lines is made by scanning both the laser frequency and the magnetic field amplitude at the same time but with different frequencies. The laser frequency is tuned slowly by modulating the chip current at a frequency f_1 of several Hz. The magnetic field intensity is modulated around the zero value with a frequency f_2, which is higher than f_1 by more than an order of magnitude. As discussed in the Introduction, modulation of the magnetic field around zero value causes a dip or a peak to be observed in the fluorescence dependence on the field. The dip or the peak is centered at $B = 0$. Thus when the magnetic field goes through zero during the slow scanning of the laser frequency, a resonance occurs. Consequently, a number f_2/f_1 of equally spaced resonances will be superimposed on the fluorescence line, each of them being positioned at a different frequency within the Doppler line (actually, the number of observed resonances may be lower than f_2/f_1, as they only appear in some parts of the scanned range). This experimental approach allows us to detect a sample of SNW resonances over the Doppler profile, and hence to study the coherent resonances' distribution, their contrast as a function of the frequency detuning within the profile of the fluorescence line, and eventually to infer the contribution of the different hf transitions.

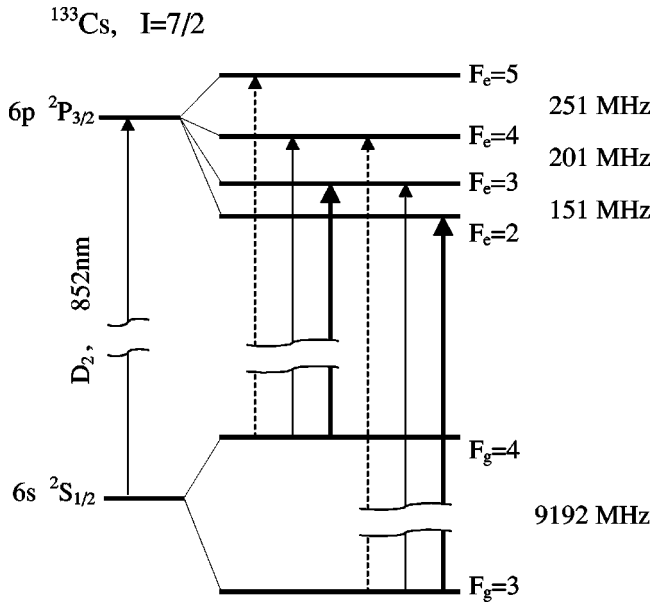

FIG. 3. Scheme of the hf transitions of the D_2 line. Three different kinds of transitions are distinguished: $F_g \rightarrow F_e = F_g - 1$ (bold), $F_g \rightarrow F_e = F_g$ (solid), and $F_g \rightarrow F_e = F_g + 1$ (dashed).

The experimental setup is shown in Fig. 2. A single-mode diode laser [full width at half maximum (FWHM) ranging from 20 to 50 MHz] tuned to the D_2 line of Cs ($\lambda = 852$ nm) is used. A sketch of the hf transitions of the D_2 line is shown in Fig. 3. The fluorescence spectrum of the D_2 Cs line consists of two lines, each resulting from three overlapping hf transitions within a Doppler profile about 375 MHz wide at room temperature [19]. Two glass cells (length 3.2 cm, diameter 2.6 cm) containing either only Cs vapor (further noted as vacuum cell) or the metal and 5 Torr of Ar (buffer gas cell) are used in the experiments.

In order to minimize the stray magnetic field, the Cs cells are placed either inside a μ-metal cylinder or in the center of three pairs of square Helmholtz coils arranged on a cubic frame (see the inset in Fig. 2); the coils are supplied by high-stability, low noise current generators. In the last case, a hollow aluminum cylinder (40 cm length, internal diameter 10 cm, thickness 4 cm) is used for additional shielding against ac stray magnetic fields. The aluminum shielding provides a factor of 20 stray magnetic field reduction at 50 Hz.

The laser light can be linearly polarized along the y axis with a ratio $|E_y|^2 : |E_x|^2 = 300:1$ for the intensities of the crossed components. A quarter-wave plate is inserted when circular polarization is needed. In this case a power ratio as good as 1.06:1 is obtained. The laser induced fluorescence of the Cs vapor is collected by a mirror in a direction perpendicular to z and is measured by a photodiode. After amplification the signal is processed by and stored in a digital scope and a computer.

III. SUBNATURAL-WIDTH RESONANCES IN THE VACUUM CELL

In this section we will discuss the dependence of the coherent resonances' contrast on the laser frequency detuning within the profiles of the fluorescence lines in the case of a vacuum cell.

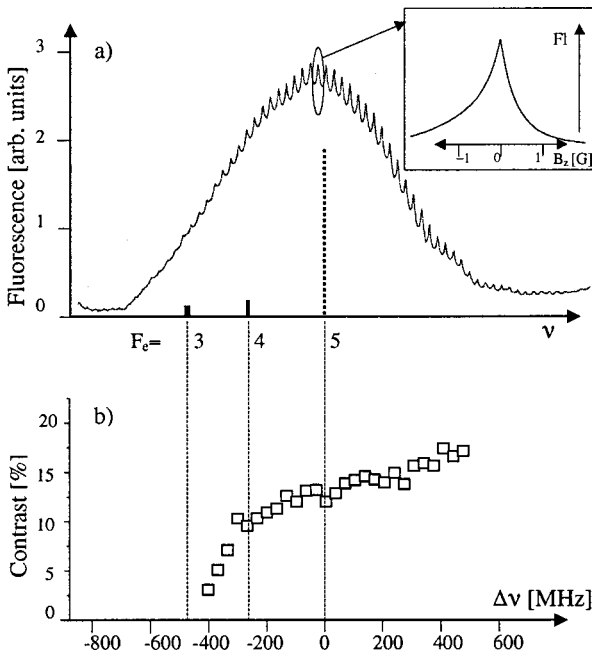

FIG. 4. (a) Bright resonances on the $F_g = 4$ fluorescence line for a linearly polarized laser beam, laser power density of 76 mW cm^{-2}, $f_1 = 8$ Hz, $f_2 = 370$ Hz depending on the detuning from the $F_g = 4 \rightarrow F_e = 5$ transition (the profile of the SNW resonance in dependence on the scanning magnetic field B_z is given in the inset). The spectrum of the hf transitions is presented by keeping the height of the lines proportional to the probability of the transitions [20]. (b) Bright resonance contrast dependence on the laser frequency detuning.

A. Linear polarization excitation of the $F_g = 4$ level

The excitation with linearly polarized light of the $F_g = 4$ ground level gives the fluorescence signal reported in Fig. 4(a). Bright narrow peaks (EIA) appear (the tops of the peaks are centered at $B = 0$), superimposed on the broad fluorescence line generated by the three hf transitions. This is a quite interesting result as, to our knowledge, observation of this kind of bright SNW resonances in Cs has not yet been reported in literature. Their linewidth strongly depends on the laser power density W. The narrowest bright resonance we have measured has a FWHM of 40 mG and has been obtained with $W = 0.02$ mW cm^{-2}. As the Zeeman splitting of the two ground hf levels in the presence of magnetic field is 0.351 kHz mG^{-1} [5], the FWHM of the bright resonance is 14 kHz, which is significantly narrower than the natural width of the transition (around 6 MHz). At very low laser power density, the width of the SNW resonances is mainly determined by the time-of-flight broadening of the ground-state levels.

We define the contrast of the SNW resonances as the ratio between the resonance and the fluorescence amplitudes. The contrast of the SNW resonances appearing in the spectrum of Fig. 4(a) is plotted in Fig. 4(b) as a function of the laser detuning.

The question is why only the EIA resonances are observed and the EIT ones are absent along the whole fluorescence line. As was noted, the two hf transitions with $F_g > F_e$ and $F_g = F_e$ should induce dark resonances, while the $F_g < F_e$ transition should give EIA resonances. The answer to this can be found by considering the transition probabilities and the level losses $\alpha = \Gamma_{F_e \to F_{g'}} / \Gamma_{F_e \to F_g}$, where $F_{g'}$ is the ground level not excited by the laser field. From Fig. 4(a) it can be seen that the probability of the $F_g = 4 \to F_e = 5$ transition is higher than the other two. Moreover, this is a so-called cycling or closed transition, as no decay is possible to the other ground-state level $F_g = 3$. The other two hf transitions are weaker and suffer losses to the $F_g = 3$ level. We calculated the losses α due to spontaneous decay to the $F_g = 3$ level and we obtained $\alpha_{(F_e=3)} = 3.0$, $\alpha_{(F_e=4)} = 0.7$, and $\alpha_{(F_e=5)} = 0$. This explains the observation of only bright resonances in the fluorescence signal of Fig. 4(a). As further evidence of this conclusion, let us point out the contrast values reported in Fig. 4(b), which increase with laser frequency, i.e., in the side corresponding to the $F_g = 4 \to F_e = 5$ transition.

This result is similar to the observations made in Rb vapor [17,21] despite the fact that the hf transitions of the D_2 line of Rb starting from a single F_g level overlap more than in the case of Cs. The contrast of SNW-EIA resonances in Cs is more than three times higher than that in Rb, which is consistent with the less overlapped hf transitions in the first case.

An explanation of the presence of the bright resonances in the $F_g \to F_e = F_g + 1$ transitions has been put forward by Renzoni *et al.* [18] for homogeneously broadened hf transitions and monochromatic laser light; the homogeneous broadening dominates in the case of experiments with atomic beams and cooled atoms. They have solved the OBE for several hf transitions of Rb and Cs and have calculated the stationary excited-state population in dependence on the magnetic field intensity B. In particular, the case of the closed $F_g = 4 \to F_e = 5$ transition in Cs has been considered and it has been shown that for weak ($0.1\ \mathrm{mW\,cm^{-2}}$) linearly polarized laser light a narrow bright resonance, superimposed on a broad line, appears around $B = 0$. Moreover, they have shown that the amplitude of the bright resonance should progressively diminish with the increasing intensity of the laser field, while a decrease of the absorption around zero magnetic field (i.e., a dip in the fluorescence) should appear within the saturated regime of the optical transition ($10\ \mathrm{mW\,cm^{-2}}$).

In order to illustrate the physical processes leading to the formation of SNW-EIA resonances, we calculated the steady-state population of the ground-state Zeeman sublevels for the $F_g = 4 \to F_e = 5$ transition by solving the OBE assuming linear polarization of the laser beam and quantization axis along the polarization vector. The calculated populations for $B_z = 0$ and $B_z = 1$ G are shown in Fig. 5(a).

The Clebsch-Gordon coefficients for the π transitions between the magnetic sublevels are presented in Fig. 5(b) [20]. It can be seen that at $B_z = 0$, the population of the $m_{F_g} = 0, \pm 1$ sublevels, which are the most coupled to the excited state levels, is significantly higher than the population of the other sublevels. At $B_z = 1$ G, the population of the other levels (less coupled to the excited state) increases at the expense of the $m_{F_g} = 0, \pm 1$ levels' population. Thus due to the redistribution of the population by the magnetic field, the population of the excited level will be higher at $B_z = 0$ than at $B_z \neq 0$, which explains the bright resonance observation at the $F_g = 4 \to F_e = 5$ transition.

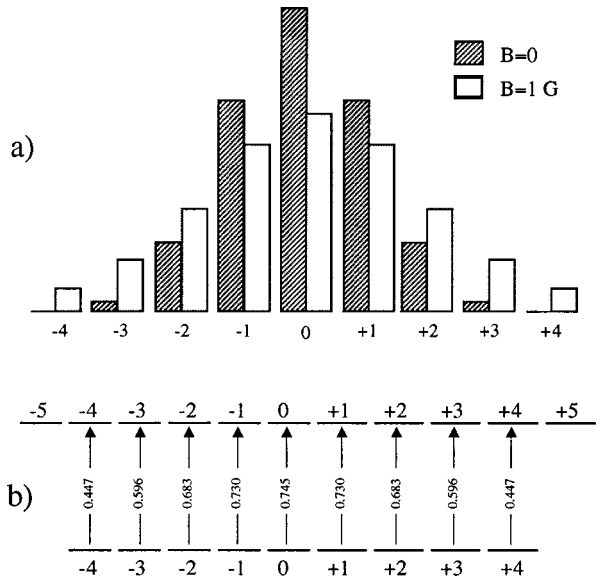

FIG. 5. (a) Illustration of the population distribution among the ground-state Zeeman sublevels of the $F_g = 4 \to F_e = 5$ transition in the absence of magnetic field and its redistribution at 1 G magnetic field. The laser is assumed to be linearly polarized and with power density $W = 1\ \mathrm{mW\,cm^{-2}}$. (b) The Clebsch-Gordon coefficients for the same transition. The population of the most coupled sublevels is decreased at $B_z \neq 0$.

Our experimental investigation confirms the result of Ref. [18] within the limit of small laser power densities but shows disagreement at large power densities. In Fig. 4(a), the coherent bright resonances are obtained with a laser power density $W = 76\ \mathrm{mW\,cm^{-2}}$, which is significantly higher than the homogeneous-broadening saturation-power-density (about $2\ \mathrm{mW\,cm^{-2}}$ [19,22]).

In Fig. 6 the experimentally measured contrast of the SNW-EIA resonances as a function of W is reported. The contrast increases with power density up to 20% at $200\ \mathrm{mW\,cm^{-2}}$.

It should be noted, though, that under our experimental conditions the main broadening of the hf transitions is the Doppler broadening, while the theory developed in [18] only considers the case of homogeneously broadened transitions. Moreover, in [18] the total population (i.e., total fluorescence) of the excited state is calculated with no evaluation of the fluorescence anisotropy.

In our theoretical consideration (see the Appendix) we have taken into account the Doppler broadening of the transitions and the spectral width of the laser light. Moreover, not only the total fluorescence, but the fluorescence along the three directions is calculated separately. The three selected directions x, y, and z are defined as shown in Fig. 2.

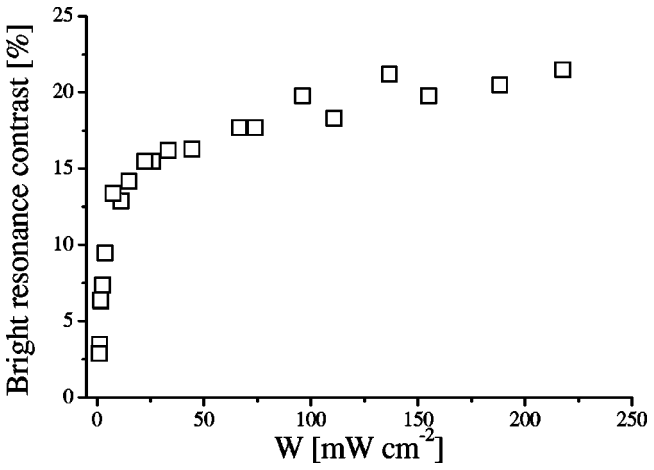

FIG. 6. Bright resonance contrast dependence on the laser power density for the fluorescence line starting from $F_g=4$, with linear polarization of the laser light. The laser frequency is tuned to the maximum of the fluorescence line and the fluorescence in the x direction is collected.

Solving the OBE under these conditions, we have found that the contrast of the SNW resonances is different in the fluorescence emitted in the three directions mentioned above [Fig. 7(a)]. The highest contrast of the SNW-EIA resonances is predicted for the fluorescence in a direction perpendicular to the polarization vector and the laser beam (x direction). The contrast of the resonances detected along the direction parallel to the polarization vector is significantly smaller. In the direction of observation parallel to the laser beam the theoretical model predicts a dip in the fluorescence centered at $B_z=0$. We have no verification of the theoretical predictions for fluorescence detected in a direction parallel to the laser beam because the windows of the cell available for our experiments were not antireflection coated and we could not separate the fluorescence in z direction from the multiple-reflected laser light. In agreement with these theoretical results when the fluorescence orthogonal to the laser beam propagation is detected, the highest contrast is observed when the fluorescence in the direction perpendicular to the polarization is measured. The contrast of the peaks on this fluorescence signal is plotted in Fig. 6. Comparing the experimental (Fig. 6) and the theoretical [Fig. 7(a)] results for the contrast of SNW-EIA resonances, a good level of agreement can be seen. The lower experimental contrast with respect to the calculated one could be due to the finite acceptance angle around the direction perpendicular to the polarization in the collection of fluorescence light.

Using our model, we have shown theoretically that the SNW-EIA resonances in the total fluorescence exist well above the homogeneous broadening saturation power density. Experimental measurement of the SNW resonances in the total fluorescence is a difficult task. For this reason we experimentally measured the SNW-EIA resonances in the transmitted laser power, which is a measure of the total laser light absorption and hence of the total fluorescence. SNW-EIA resonances in the transmitted laser beam were observed for laser power densities up to 350 mW cm^{-2}, which was the maximum density available in our experiment. Consequently, when the Doppler broadening of the hf transition and the spectral width of the laser light are taken into consideration, there is an agreement between the theoretical and experimental results concerning the case of the total fluorescence. The comparison of the experimental profiles of SNW-EIA resonances with the theoretical ones shows a good level of agreement, which is illustrated in Fig. 7(b).

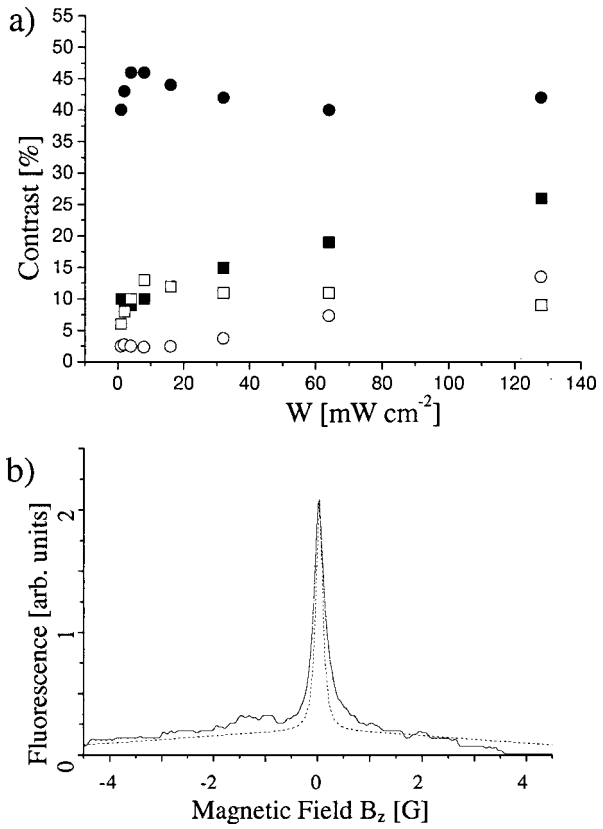

FIG. 7. (a) Theoretical calculation of the SNW resonances' contrast in dependence on the power density, for excitation of $F_g=4$ with a linearly polarized laser beam. The laser light FWHM is 50 MHz. The four plots report the total fluorescence (■) and the fluorescence emitted in the x (●), y (○), and z (□) direction, respectively. (b) Comparison between the experimental SNW resonance line shape at $W=4$ mW cm^{-2} (solid line) and the theoretical one (dashed line).

As a last remark, we will note that in a similar σ^+, σ^- Hanle configuration experiment with a laser beam of only a few mW cm^{-2} power density, in [20] no coherent resonances around $B=0$ were observed for the $F_g \rightarrow F_e=F_g+1$ transitions and in particular for the $F_g=4 \rightarrow F_e=5$ transition. The theoretical model developed there also does not show narrow resonances for these kinds of transitions.

B. Linear polarization excitation of the $F_g=3$ level

When the $F_g=3$ level is excited, coherent dark resonances are observed at $B_z=0$. The excitation with linearly polarized light of the $F_g=3$ level gives the fluorescence signal reported in Fig. 8(a).

For low power density ($W=0.08$ mW cm^{-2}), the FWHM of the resonance is 45 mG and it increases up to 460

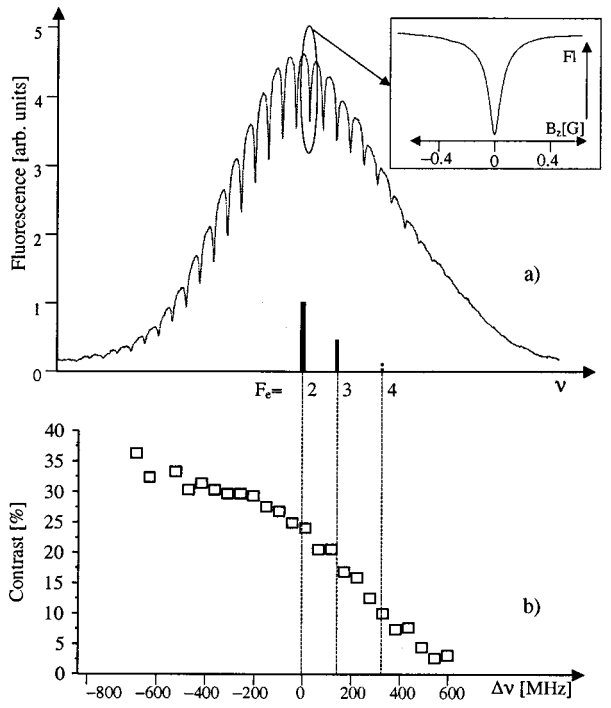

FIG. 8. (a) Dark resonances on the $F_g=3$ fluorescence line for a linearly polarized laser beam, laser power density of 0.15 mW cm^{-2}, $f_1=6$ Hz, $f_2=370$ Hz depending on the detuning from the $F_g=3\rightarrow F_e=2$ transition (the profile of the SNW resonance in dependence on the magnetic field B_z is given in the inset). The spectrum of the transition is presented in the same way as in Fig. 4. (b) Dark resonance contrast in dependence on the laser frequency detuning.

mG for $W=10$ mW cm^{-2}. The interpretation can be obtained according to the previous scheme (see Sec. III A). The probability of the $F_g=3\rightarrow F_e=2$ transition, which is a closed transition, is now the highest, but, unlike in the previous case, this transition leads to dark resonances (see Fig. 1). In addition, the calculation of the losses α gives the following values: $\alpha_{(F_e=2)}=0$, $\alpha_{(F_e=3)}=0.3$, and $\alpha_{(F_e=4)}=1.4$. This shows that the other two transitions suffer strong losses, leading to the observed result. In Fig. 8(b) the contrast of the resonances is reported. As in the case of the bright resonances, the contrast of the dark resonances depends on the detuning of the laser frequency within the fluorescence profile. It is higher the closer the tuning is to the $F_g=3\rightarrow F_e=2$ transition, i.e., in the red wing of the Doppler profile.

It should be pointed out that the dark resonances have also been obtained by Theobald *et al.* [20] by irradiating a Cs atomic beam by linearly polarized laser light. The existence of only the dark resonances was confirmed there theoretically. The influence of coherent effects at the $F_g=3\rightarrow F_e=2$ transition on the saturated absorption spectra of Cs is discussed in [23].

IV. SUBNATURAL-WIDTH RESONANCES IN A BUFFER GAS CELL

In this section we present experimental and theoretical examination of the influence of buffer gas on the SNW resonances at the Cs D_2 line.

In previous works dealing with coherent resonances in degenerate two-level systems, alkali atoms were investigated either in atomic beams [9,20] or confined in vacuum cells, through detection of fluorescence or transmitted light [11,15–17,21].

Investigations of the potential of the nonlinear Faraday rotation (NLFR) in degenerate two-level systems to measure weak magnetic field have mainly been performed in evacuated cells containing alkali atoms [13,14,24], while few works deal with NLFR in buffer gas cells. It was shown that the NLFR resonances in samarium are very sensitive to atomic collisions [25]. In particular, it was shown that Ar or He buffer gas at pressures of the order of 0.1 Torr decreases the amplitude of the NLFR resonances in samarium vapor by an order of magnitude. In another experiment with 3 Torr Ne buffer gas and optically dense Rb vapor (obtained by heating of the Rb cell) [26] it was demonstrated that the amplitude of the NLFR strongly decreases when the cell temperature approaches 27 °C.

Both the NLFR studied by other groups and the SNW resonances described in this paper are related to the ground-state Zeeman-sublevel coherence. In the case of NLFR experiments one measures the rotation of the linear polarization of the polarized light propagating in the direction of the magnetic field and transmitted through the sample. On the other hand, we examine the SNW resonances in the laser induced fluorescence in different geometries, concerning the polarization of the laser light, the orientation of the applied magnetic field, and the detection direction. We report here the observation of the influence of buffer gas on the SNW coherent resonances in the fluorescence in a degenerate two-level system.

In the experimental setup, the vacuum cell is replaced by a Cs cell with Ar, while the rest of the apparatus is not modified (Fig. 2).

The buffer gas may influence the incoherent and coherent interactions of the light with atoms. Concerning the incoherent interaction, as shown by de Tomasi *et al.* [19], a strong modification of the fluorescence spectrum of the D_2 line is observed in the buffer gas cell as a function of the laser intensity due to optical pumping. At low laser power the spectrum consists of two well-resolved fluorescence lines arising from the two ground-state levels $F_g=3$ and $F_g=4$. However, when the laser power is increased, fluorescence in the whole region between the two lines appears. For a laser frequency tuned into resonance with one hf transition, hyperfine optical pumping [27] accumulates the population into the state noncoupled with the radiation and a fluorescence signal decrease is observed. When the laser frequency is tuned to a position halfway between the two fluorescence lines, the hf optical pumping into the $F_g=3$ and $F_g=4$ levels is equal and leads to maximum absorption, hence, to maximum fluorescence.

Using a 5 Torr Ar buffer gas cell in our experiment, we observed a modification of the fluorescence similar to that reported in [19]. The purpose of our work was, however, to take a further step and investigate the influence of the buffer gas on the coherent effects, i.e., to discover whether narrow resonances like those in Figs. 4 and 8 exist in the case of

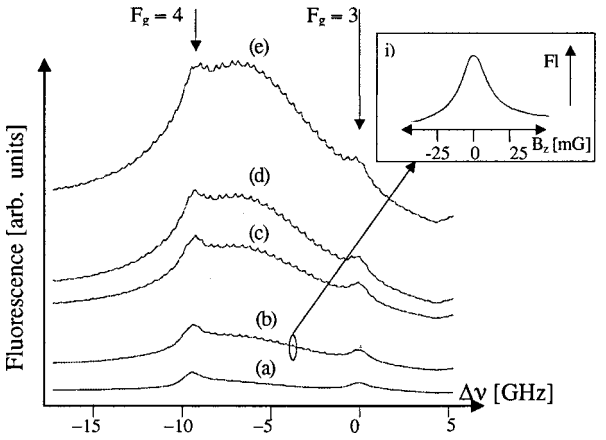

FIG. 9. Coherent resonances on the spectrum of the D_2 line in a Cs cell with 5 Torr Ar for circular polarization of the laser beam, $f_1=10$ Hz and $f_2=513$ Hz depending on the detuning from the maximum of the fluorescence line starting from $F_g=3$. The curves are for power densities as follows: (a) 5 mW cm^{-2}, (b) 19 mW cm^{-2}, (c) 40 mW cm^{-2}, (d) 57 mW cm^{-2}, and (e) 84 mW cm^{-2}. The profile of the SNW resonance depending on the magnetic field B_z is given in the inset.

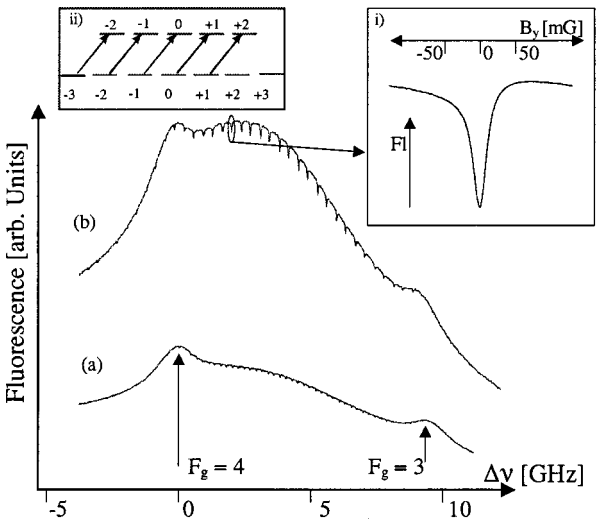

FIG. 10. Coherent resonances on the spectrum of the D_2 line for a magnetic field applied in the y direction, circular polarization of the laser beam, Cs cell with 5 Torr Ar, $f_1=0.3$ Hz depending on the detuning from the maximum of the fluorescence line starting from $F_g=4$, (a) $f_2=20$ Hz and $W=17$ mW cm^{-2} and (b) $f_2=12$ Hz and $W=47$ mW cm^{-2}. Inset (i): dark resonance profile in dependence on the magnetic field B_y. Inset (ii): schematic presentation of the $F_g>F_e$ transitions.

buffer gas and to examine their sign and the distribution of their contrast over the entire (more than 9.2 GHz) broad profile of the fluorescence. As in the case of vacuum cell, together with the slow scan of the diode laser frequency, a fast magnetic field tuning was applied, which provides registration of the SNW resonances over the entire fluorescence profile.

The experiments performed by us with linear and circular polarization showed that SNW resonances are observed only when the Cs cell is illuminated by circularly polarized laser light. In Fig. 9 the fluorescence spectra obtained are shown. SNW peaks can be seen superimposed on the profile of the fluorescence. The tops of the peaks are centered at $B_z=0$. In the inset of Fig. 9 one of the resonances is shown in detail. It is worth noting the peculiar fact that only peaks in the fluorescence are observed and their amplitude changes very little in the entire region between the two fluorescence lines. This deserves consideration because here six hf transitions with $F_g<F_e$ and $F_g\geqslant F_e$ contribute to the formation of the fluorescence profile, i.e., SNW resonances of different signs and contrast could be expected.

We also performed experimental investigation for the case of circularly polarized laser light illuminating the Cs vacuum cell. We observed that for transitions with $F_g\rightarrow F_e=F_g$, F_g-1 peaks are present in the fluorescence. The same result was previously reported in Rb [21] where the observation of the peaks in the fluorescence was attributed to the influence of some residual magnetic field perpendicular to the laser beam propagation direction.

In order to examine the SNW resonances with circular polarization under well-defined experimental conditions, the buffer gas cell was irradiated by a circularly polarized laser beam propagating in the z direction and at the same time, magnetic field B_y was applied and scanned around zero value (see Fig. 10).

For quantization axis in the z direction and $B_y=0$, Zeeman optical pumping to the $m_{F_g}=+2,+3$ sublevels takes place for the $F_g=3\rightarrow F_e=2$ transition, which is taken as an example of a $F_g>F_e$ transition [see inset (ii) in Fig. 10]. Due to the optical pumping to magnetic sublevels not interacting with the laser field, the fluorescence has a minimum at $B_y=0$. When $B_y\neq 0$, the population from $m_{F_g}=+2,+3$ is redistributed to the other sublevels of the $F_g=3$ state, increasing the absorption and hence the fluorescence. Therefore when B_y is scanned around zero value, dips in the fluorescence are expected for $F_g\geqslant F_e$ transitions.

On the contrary, in the case of $F_g\rightarrow F_e=F_g+1$ transitions and circularly polarized beam peaks in the fluorescence centered at $B_y=0$ should be expected. Peaks in the fluorescence have been observed for $F_g\rightarrow F_e=F_g+1$ transitions in a vacuum Rb cell for B_y magnetic field scanning [28]. However, when scanning B_y, in our experiment only dips in the fluorescence are observed (Fig. 10).

As shown in Sec. III, in the case of a vacuum cell the two closed hf transitions play the most important role in the formation of the coherent resonances and the contributions of the open transitions are not considered. However, as discussed in [19], the role of the open transitions is essential for producing the broad central part of the fluorescence profile in the case of a buffer gas cell and high laser power densities. The contrast of the coherent resonances obtained in our experiment is the highest exactly in that broad fluorescence interval between the two fluorescence lines of the Cs D_2 line. That is why we have to consider all hf transitions when discussing the buffer gas cell case.

As mentioned above, population accumulation on a certain Zeeman sublevel is essential for the observation of narrow structures in degenerate systems. Therefore we will con-

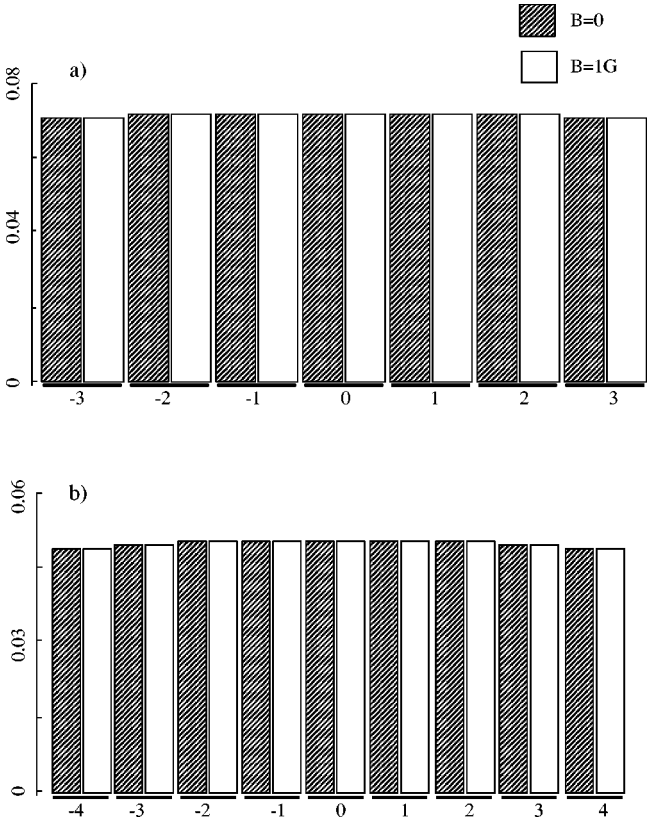

FIG. 11. Population distribution among the Zeeman sublevels of (a) $F_g=3$ and (b) $F_g=4$ levels for linear polarization of the laser light and power density $W=80$ mW cm^{-2}. The frequency of collisions with buffer gas atoms, which lead to redistribution of the population of the excited-state Zeeman sublevels, is 90 MHz.

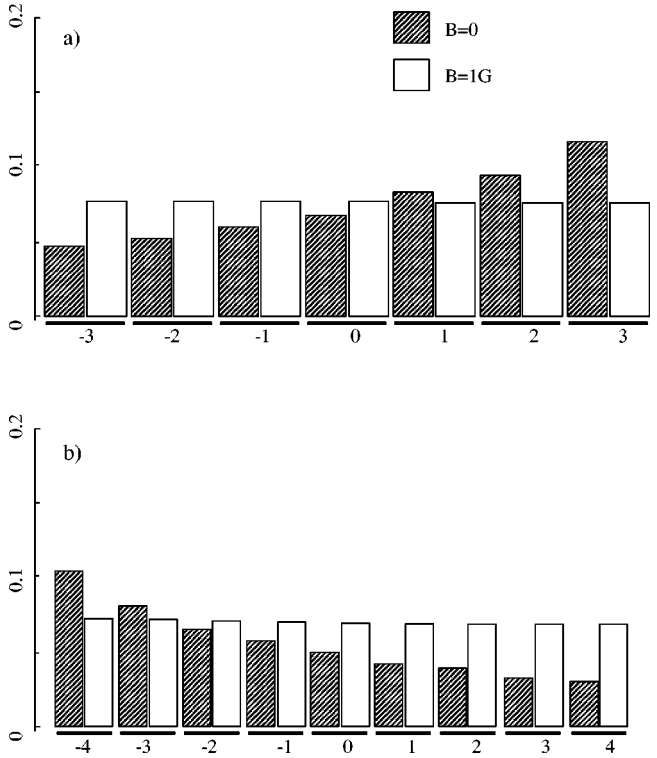

FIG. 12. Population distribution among the Zeeman sublevels of (a) $F_g=3$ and (b) $F_g=4$ levels for circular polarization of the laser light and power density $W=80$ mW cm^{-2}. The collision rate responsible for the redistribution of population in the excited-state sublevels is the same as for Fig. 11.

sider the accumulation in the two cases of linearly and of circularly polarized light.

First, the case of linearly polarized light will be discussed. Taking into account the probability of the transitions between the Zeeman sublevels [20], it can be concluded that no significant optical pumping occurs at $B=0$. Thus, the application of a magnetic field cannot create the necessary conditions for observation of a narrow structure by redistributing the population among the Zeeman sublevels. This conclusion is fully supported by our theoretical calculation of the populations of the Zeeman sublevels of the two ground-state hf levels, shown in Fig. 11 (see the Appendix). No difference can be seen between the populations of the Zeeman sublevels for $B_y=0$ and $B_y=1$ G.

The opposite situation applies to the case of a circularly polarized laser beam. In this case, for quantization axis along the z direction, the Zeeman optical pumping due to the three hf transitions ($F_g=3\rightarrow F_e=2,3,4$) leads to a strong accumulation of atoms on the $m_{F_g}=+3$ sublevel for σ^+ polarization. Once on this magnetic sublevel, atoms cannot be excited any more by the laser radiation.

Concerning the $F_g=4$ level, in the presence of intense circularly polarized laser light (σ^+), most of the atoms will circulate in the $m_{F_g}=4\rightarrow m_{F_e}=5$ transition. Due to collisions with the buffer gas atoms, the Cs atoms accumulated on the $m_{F_e}=5$ can be redistributed among the other Zeeman sublevels of the $F_e=5$ level (see the Appendix). Taking into account the difference in probability of the transitions between the Zeeman sublevels, it could be expected that under excitation with σ^+ polarization, the redistribution of the population to different sublevels of the $F_e=5$ will lead to the accumulation of many atoms on $m_{F_g}=-4$. This level has the lowest probability for σ^+ excitation.

Consequently, unlike the linearly polarized laser beam case, a significant accumulation of the population on a single magnetic sublevel of the two ground-state hf levels takes place for circular polarization. It should be pointed out that for the two ground state levels, the accumulation of the atoms on $m_{F_g}=-4$ and $m_{F_g}=+3$ leads to the lowest level of fluorescence. Hence, as a result of this accumulation, if the magnetic field perpendicular to the laser beam propagation is scanned around zero value, SNW-EIT resonances can be expected and this is observed experimentally.

This discussion is supported by our calculations of the population of the magnetic sublevels of the $F_g=3$ and $F_g=4$ levels under σ^+ circularly polarized light (see the Appendix). The accumulation of the population on the $m_{F_g}=+3$ and $m_{F_g}=-4$ at $B=0$ can be clearly seen (Fig. 12). At $B=1$ G the atomic population is redistributed almost equally among all Zeeman sublevels. Thus the experimental observation of SNW-EIT resonances with circularly polarized laser light and a scan of B_y around $B_y=0$ is in agree-

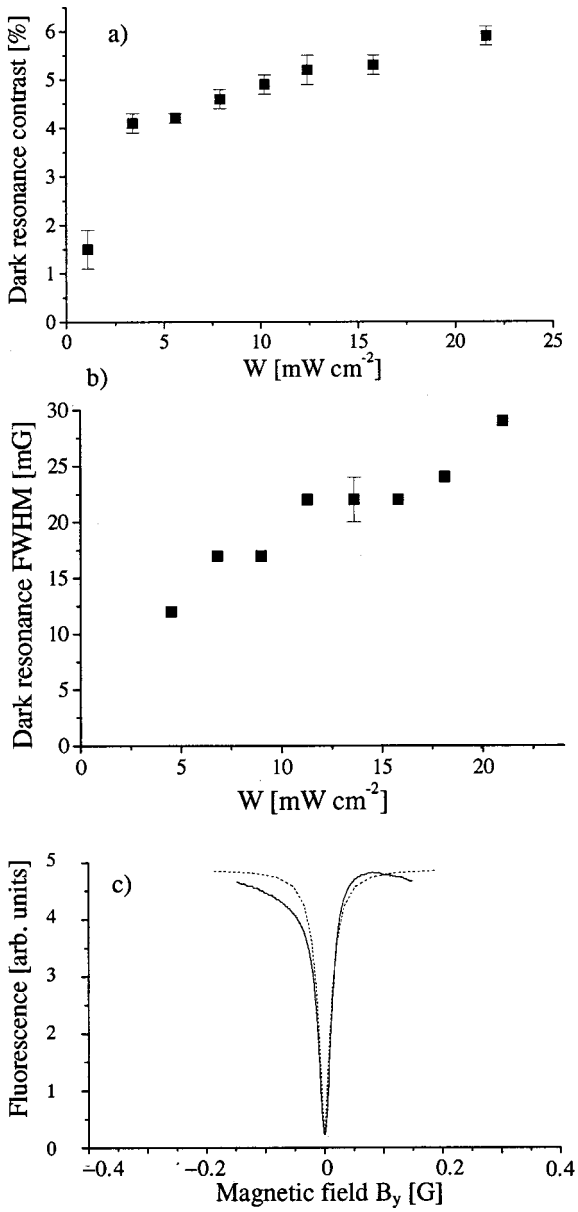

FIG. 13. Contrast (a) and FWHM (b) of the dark resonances in dependence on the laser power density. The resonances are registered in a 5 Torr Ar buffer gas cell when scanning B_y and when the laser light with circular polarization is tuned to a frequency halfway between the two fluorescence lines. (c) Comparison between the experimental curve of the SNW resonance at $W=47$ mW cm^{-2} (solid line) and the theoretical curve (dashed line).

ment with the theoretical model. The same model accounts for the peaks observed in the conditions of Fig. 9, provided that a small (residual) magnetic field is considered in the y direction, thus also confirming the interpretation given in [21].

It is known [9] that the width and the contrast of the SNW resonances depend on the laser power density. The dependence of the dark resonance contrast on the laser power density is shown in Fig. 13(a) for laser frequency tuned to a position halfway between the two fluorescence lines. It can be seen that the contrast of the coherent resonances in the buffer gas cell is smaller than that in the vacuum cell. In the vacuum cell the contrast of the dark resonance is about 40% and that of the bright resonance about 15% for excitation with linearly polarized light with a power density of 25 mW cm^{-2}.

It is worth noting the difference in the FWHM of the Cs SNW resonances in vacuum and in buffer gas cells. In the first case, the FWHM of the coherent dips observed in the fluorescence line starting from $F_g=3$ is 460 mG for a power density of 10 mW cm^{-2} (see Sec. III). As can be seen from Fig. 13(b), where the dark resonances' FWHM is plotted in dependence on the laser power density, at equal power densities (10 mW cm^{-2}) the FWHM in the buffer gas cell is 18 mG, which is about 25 times narrower than in the case of the vacuum cell. Collisions with the buffer gas atoms cause a reduction of the mean free path of the Cs atoms, thus prolonging the time-of-flight, and hence producing a significant reduction of the FWHM.

For similar conditions, an example of theoretical and experimental profiles is presented, Fig. 13(c), which shows a good level of agreement. Strong narrowing of the CPT resonances in three-level systems in case of Cs with buffer gas has been demonstrated in [5]. Thus, though in general the contrast of the SNW-EIT resonances in buffer gas is lower than in a vacuum cell, the comparison of the contrast at equal FWHM in both cases is in favor of the buffer gas case. Experimental and theoretical investigations to compare the signal-to-noise ratio in both cases are in progress.

Another advantage of the buffer gas for practical applications of the SNW resonances is the significantly less critical requirements to the laser frequency stability with respect to drifts, due to the much larger width of the fluorescence profile (about 9 GHz) than in the case of a vacuum cell (about 400 MHz).

Our results are in agreement with those on the influence of the buffer gas on the dark resonance observed when two ground-state hf levels are coupled to a common excited hf level by two laser frequencies, performed in [29]. There it is shown that destruction of the dark resonance takes place when optical pumping depletes the population of the levels involved in the formation of the dark resonance. However, when the optical pumping increases the population of these levels, the dark resonances exist at much higher buffer gas pressures.

V. CONCLUSION

Subnatural-width coherent resonances have been observed in hf transitions of the D_2 line of Cs both in vacuum and buffer gas cells. In the case of Cs vapor contained in a vacuum cell at room temperature, due to the significant population losses for the open transitions, the two closed transitions determine the sign of the observed coherent resonances at the two fluorescence lines arising from $F_g=3$ and $F_g=4$ levels. For the $F_g=3$ fluorescence line, the closed transition is the $F_g=3\rightarrow F_e=2$ (Λ system), which corresponds to observed dark resonances in the fluorescence for the linearly polarized laser beam. For the $F_g=4$ fluorescence line, the closed transition is $F_g=4\rightarrow F_e=5$ (V system),

which is the reason for the observation of bright resonances with linear polarization. While dark resonances at hf transitions of the D_2 line have been observed by other authors, the SNW bright resonances at the $F_g=4\rightarrow F_e=5$ transition are reported here. Under the conditions of our experiment, high-contrast (up to 20%) bright resonances were registered at 200 $\mathrm{mW\,cm^{-2}}$ power density, which disagrees with the recently developed theory explaining the bright resonances at homogeneously broadened $F_g\rightarrow F_e=F_g+1$ hf transitions. Taking into account the Doppler broadening and the linewidth of the laser light, our theoretical model confirms the resonance observation at high power densities.

In buffer gas the hf optical pumping is enhanced, which leads to a decrease and destruction of the coherent resonances. However, this can be significantly overcome by using high power density and by tuning the laser frequency between the two fluorescence lines. Our experimental investigations show that coherent resonances are observed only with circular polarization of the laser beam, which is in agreement with the proposed theoretical model. The contrast of the coherent resonances does not change significantly along the broad part of the fluorescence profile between the two fluorescence lines. This makes the requirement to the laser frequency drift for observation of SNW resonances less critical, which is an advantage of using buffer gas cells for practical applications. The narrowing of the SNW resonances in the buffer gas cell has also a potential for application. Investigations are in progress to compare the signal-to-noise ratio at equal FWHM of the SNW resonances in vacuum and in buffer gas cells.

The fact that the coherent resonances have a much narrower linewidth than the natural linewidth of the optical transitions is very interesting for high-resolution spectroscopy and for metrological applications. It should be noted that width and contrast of the SNW resonances are very sensitive to additional magnetic fields, which makes their application for building simple and precise magnetometers attractive.

ACKNOWLEDGMENTS

C.A., S.C., and Y.D. are grateful to their colleagues from Professor L. Moi's Laboratory for their hospitality during the common experiments at the University of Siena. They would also like to thank Professor E. Arimondo and Dr. F. Renzoni for the very helpful discussions. They would also like to acknowledge the Bulgarian NCSR for partial support of the work (Grant No. F-1005/00). The authors thank Professor Alzetta from the University of Pisa for his continuous help and Professor Minguzzi for his assistance. The experiments were realized with the technical help of M. Badalassi, C. Stanghini, A. Barbini, A. Pifferi, and E. Corsi. K.N. thanks the Russian Foundation for Basic Research (RFBR, Grant No. 01-02-17433) for partial support of the work.

APPENDIX

The equation for the density matrix $\hat{\rho}$ is taken in the form

$$i\hbar\left(\frac{\partial}{\partial t}+\mathbf{v}\cdot\frac{\partial}{\partial\mathbf{r}}+\hat{\Gamma}\right)\hat{\rho}=[H_0,\hat{\rho}]+[V_B+V,\hat{\rho}], \quad \text{(A1)}$$

where $\hat{\Gamma}$ is the operator of atom relaxation, H_0 is the Hamiltonian of the free atom, $V_B=\mu g\mathbf{F}\cdot\mathbf{B}$ is the interaction potential with the magnetic field $\mathbf{B}$ (μ is the Bohr magneton, g is the Landé factor, and $\mathbf{F}$ is the total angular momentum of the atom), and $V=-\mathbf{d}\cdot\mathcal{E}$ is the potential of the electric dipole interaction with the electric field of a monochromatic wave

$$\mathcal{E}=\mathbf{E}e^{-i\omega t+i\mathbf{k}\cdot\mathbf{r}}+\text{c.c.} \quad \text{(A2)}$$

We consider an atom with a set of excited levels $\{|e\rangle=|F_e,M_e\rangle\}$ with energies $\{E_e\}$ and a set of ground states $\{|g\rangle=|F_g,M_g\rangle\}$ with energies $\{E_g\}$. The excited hf states are assumed to have a separation smaller than the Doppler width. For the D_2 line of alkali atoms, there are four excited hf states and two ground hf states. We assume that the laser frequency is close to the $g\rightarrow e$ transition

$$\left|\frac{E_e-E_g}{\hbar}-\omega\right|\ll\omega, \quad \text{(A3)}$$

so that a rotating wave approximation can be applied.

In this approximation, with the quantization axis along the magnetic field direction and for the nondiagonal elements of the density matrix, Eq. (A1) can be written in the form

$$\left[\Gamma+i\mathbf{k}\cdot\mathbf{v}-i\omega+i\frac{E_e-E_g}{\hbar}+i\frac{\mu}{\hbar}(g_eM_e-g_gM_g)B\right]\rho_{eg}$$
$$=-\frac{i}{\hbar}\left[\sum_{g'}V_{eg'}\rho_{g'g}-\sum_{e'}\rho_{ee'}V_{e'g}\right], \quad \text{(A4)}$$

where Γ is the homogeneous half-width of the transition. In this equation we neglect the time derivative because the transit time of the atom across the laser beam is much greater than the spontaneous decay time.

The matrix element of the electric dipole interaction is

$$V_{eg}=-\sum_{\sigma}(-1)^{\sigma}\langle e|d_{-\sigma}|g\rangle E_{\sigma}, \quad V_{ge}=V_{eg}^{*}. \quad \text{(A5)}$$

Here d_σ and E_σ are the circular components ($\sigma=-1,0,+1$) of the dipole and the electric field vectors, respectively. The explicit form for the matrix element of the dipole moment is

$$\langle F_e,M_e|d_\sigma|F_g,M_g\rangle$$
$$=d(-1)^{F_e-M_e+J_e+I+F_g+1}\sqrt{(2F_e+1)(2F_g+1)}$$
$$\times\begin{Bmatrix}J_e & F_e & I\\ F_g & J_g & 1\end{Bmatrix}\begin{pmatrix}F_e & 1 & F_g\\ -M_e & \sigma & M_g\end{pmatrix}. \quad \text{(A6)}$$

Here d is the reduced matrix element of the dipole moment for the $J_g\rightarrow J_e$ transition, I is the nuclear momentum, and J_e,J_g are the electron momenta in the excited and ground states, respectively.

Substituting the nondiagonal elements of the density matrix from Eq. (A4) into the equations for the density matrix elements of the excited and ground states, we obtain

$$\frac{\partial}{\partial t}\rho_{ee'}+\rho_{ee'}\left[\gamma+\Gamma_m+i\frac{E_e-E_{e'}}{\hbar}+i\frac{\mu}{\hbar}(g_eM_e-g_{e'}M_{e'})B\right]-\delta_{e,e'}\frac{\Gamma_m}{N_e}\sum_{e_1}\rho_{e_1e_1}=\sum_{g,g'}U_{e,e';g,g'}\rho_{gg'}-\sum_{e_1,e_1'}U_{e,e;e_1,e_1'}\rho_{e_1e_1'} \tag{A7}$$

and

$$\frac{\partial}{\partial t}\rho_{gg'}+\left[i\frac{E_g-E_{g'}}{\hbar}+i\frac{\mu}{\hbar}(g_gM_g-g_{g'}M_{g'})B\right]\rho_{gg'}=\left(\frac{\partial}{\partial t}\rho_{gg'}\right)_S+\sum_{e,e'}U_{g,g';e,e'}\rho_{ee'}-\sum_{g_1,g_1'}U_{g,g';g_1,g_1'}\rho_{g_1g_1'}, \tag{A8}$$

respectively, where the elements of the matrix U are

$$U_{e,e';g,g'}=\frac{1}{\hbar^2}(Z^*_{e'g}+Z_{eg'})V_{eg}V_{g'e'}, \tag{A9}$$

$$U_{g,g';e,e'}=\frac{1}{\hbar^2}(Z^*_{e'g}+Z_{eg'})V_{ge}V_{e'g'},$$

$$U_{e,e';e_1,e_1'}=\frac{1}{\hbar^2}\sum_g(\delta_{e',e_1'}Z^*_{e'g}V_{eg}V_{ge_1}+\delta_{e,e_1}Z_{eg}V_{e_1'g}V_{ge'}), \tag{A10}$$

$$U_{g,g';g_1,g_1'}=\frac{1}{\hbar^2}\sum_e(\delta_{g',g_1'}Z_{eg'}V_{ge}V_{eg_1}+\delta_{g,g_1}Z^*_{eg}V_{g_1'e}V_{eg'}) \tag{A11}$$

with

$$Z_{eg}=\left[\Gamma+i\mathbf{k}\cdot\mathbf{v}-i\omega+i\frac{E_e-E_g}{\hbar}+i\frac{\mu}{\hbar}(g_eM_e-g_gM_g)B\right]^{-1}. \tag{A12}$$

In Eq. (A7), γ is the spontaneous decay rate, Γ_m is the rate of collision mixing between the Zeeman sublevels of the excited states, and $N_e=\Sigma_{F_e}(2F_e+1)$ is the total number of excited state sublevels. In our model we assume that the collisions with the noble gas atoms are able to destroy any coherence between the Zeeman sublevels of the excited states, but they cannot disturb the coherence in the Zeeman ground states because the angular momenta of the latter are composed only by electron and nuclear spins.

In Eq. (A8), the term of spontaneous repopulation of the ground states has the following explicit form

$$\left(\frac{\partial}{\partial t}\rho_{gg'}\right)_S=\delta_{F_g,F_g'}\frac{\gamma}{d^2}\times\sum_{\sigma,F_e,M_e,F_e',M_e'}\delta_{F_e,F_e'}\langle F_g,M_g|d_\sigma|F_e,M_e\rangle\times\langle F_e',M_e'|d_{-\sigma}|F_g',M_g'\rangle\rho_{ee'}. \tag{A13}$$

Equations (A7) and (A8) are obtained for a system of coordinates with the z axis along the magnetic field direction, so the electric field vector components have to be calculated in this system of coordinates. This can be done by means of the transformation

$$E_{\sigma'}=\sum_\sigma D^{1*}_{\sigma,\sigma'}(0,\theta,\phi)E^L_\sigma, \tag{A14}$$

where the E^L_σ are the circular components of the electric field vector in the laboratory frame; $D^1_{\sigma,\sigma'}(0,\theta,\phi)$ are the Wigner D-functions, and θ and ϕ define the polar and azimuth angles of the magnetic field direction.

Equations (A7) and (A8) are also generalized for the case of finite width of the radiation spectrum $I(\omega)$. For that one substitutes the Z_{eg} function with

$$\frac{\int Z_{eg}I(\omega)d\omega}{\int I(\omega)d\omega}. \tag{A15}$$

In order to compare this theoretical model with the experimental results, the equations (A7) and (A8) are solved numerically. For the case of a vacuum cell we assume $\Gamma=\gamma/2$, $\Gamma_m=0$. In this case Eqs. (A7) and (A8) are solved along the atom trajectory crossing the laser beam. The intensity across the laser beam is assumed to have a Gaussian shape.

The fluorescence intensity in the **n** direction is given by the equation

$$I_f(\mathbf{n})\propto\langle[\mathbf{n}\times\mathbf{d}]^2\rho\rangle_{e,t,v}. \tag{A16}$$

Here $\langle\,\rangle_{e,t,v}$ means averaging over: all excited states of the atom; the Maxwell velocity distribution along the wave propagation direction **k**, as well as in the directions perpendicular to the laser beam; and the transit time of the atom through the laser beam.

For the case of a buffer gas cell we assume that $\Gamma=\Gamma_m$ and here Γ is the linewidth broadened by collisions with the buffer gas atoms. In this case no averaging over velocity is needed if the laser frequency is tuned to a position halfway between the two hf ground states.

[1] G. Alzetta, A. Gozzini, L. Moi, and G. Orriols, Nuovo Cimento Soc. Ital. Fis. **36B**, 5 (1976); G. Alzetta, L. Moi, and G. Orriols, Nuovo Cimento, **52B**, 209 (1979).
[2] E. Arimondo, Prog. Opt. **35**, 257 (1995), and references therein.
[3] S.E. Harris, Phys. Today **50**, 36 (1997).
[4] A. Aspect, E. Arimondo, R. Kaiser, N. Vansteenkiste, and C. Cohen-Tannoudji, Phys. Rev. Lett. **61**, 826 (1988).
[5] A. Nagel, L. Graf, A. Naumov, E. Mariotti, V. Biancalana, D. Meschede, and R. Wynands, Europhys. Lett. **44**, 31 (1998); R. Wynands and A. Nagel, Appl. Phys. B: Lasers Opt. **B68**, 1 (1999).
[6] S.E. Harris, J.E. Field, and A. Kasapi, Phys. Rev. A **46**, R29 (1992).
[7] K. Bergmann, H. Theuer, and B.W. Shore, Rev. Mod. Phys. **70**, 1003 (1998).
[8] L.V. Hau, S.E. Harris, Z. Dutton, and C.H. Behroozi, Nature (London) **397**, 594 (1999).
[9] F. Renzoni, W. Maichen, L. Windholz, and E. Arimondo, Phys. Rev. A **55**, 3710 (1997).
[10] F. Renzoni and E. Arimondo, Europhys. Lett. **46**, 716 (1999).
[11] A.M. Akulshin, S. Barreiro, and A. Lezama, Phys. Rev. A **57**, 2996 (1998).
[12] V.S. Smirnov, A.M. Tumaikin, and V.I. Yudin, Sov. Phys. JETP **69**, 913 (1989); A.B. Taichenachev, A.V. Tumaikin, V.I. Yudin, and G. Nienhuis, *ibid.* **81**, 224 (1995); A.B. Taichenachev, A.V. Tumaikin, and V.I. Yudin, Zh. Éksp. Teor. Fiz., **110**, 1727 (1996) [Sov. Phys. JETP **83**, 94 (1996)].
[13] D. Budker, V. Yashchuk, and M. Zolotorev, Phys. Rev. Lett. **81**, 5788 (1998).
[14] D. Budker, D.F. Kimball, S.M. Rochester, V.V. Yashchuk, and M. Zolotorev, Phys. Rev. A **62**, 043403 (2000).
[15] A. Lezama, S. Barreiro, and A.M. Akulshin, Phys. Rev. A **59**, 4732 (1999).
[16] A. Lezama, S. Barreiro, A. Lipsich, and A.M. Akulshin, Phys. Rev. A **61**, 013801 (1999).
[17] Y. Dancheva, G. Alzetta, S. Cartaleva, M. Taslakov, and Ch. Andreeva, Opt. Commun. **178**, 103 (2000).
[18] F. Renzoni, C. Zimmermann, P. Verkerk, and E. Arimondo, J. Opt. B: Quantum Semiclassical Opt. **3**, S7 (2001).
[19] F. de Tomasi, M. Allegrini, E. Arimondo, G.S. Agarwal, and P. Ananthalakshmi, Phys. Rev. A **48**, 3820 (1993).
[20] G. Theobald, N. Dimarca, V. Giordano, and P. Cerez, Opt. Commun. **71**, 256 (1989).
[21] G. Alzetta, S. Cartaleva, Y. Dancheva, Ch. Andreeva, S. Gozzini, L. Botti, and A. Rossi, J. Opt. B: Quantum Semiclassical Opt. **3**, 181 (2001).
[22] H. Hori, Y. Kitayama, M. Kitano, and T. Yabuzaki, IEEE J. Quantum Electron. **QE19**, 169 (1983); D. A. Steck, http://www.ph.utexas.edu/ ~quantopt
[23] O. Schmidt, K.-M. Knaak, R. Wynands, and D. Meschede, Appl. Phys. B: Lasers Opt. **B59**, 167 (1994).
[24] A. Weis, J. Wurster, and S.I. Kanorsky, J. Opt. Soc. Am. B **10**, 716 (1993).
[25] L.M. Barkov, D.A. Melik-Pashayev, and M.S. Zolotorev, Opt. Commun. **70**, 467 (1989).
[26] V.A. Sautenkov, M.D. Lukin, C.J. Bednar, I. Novikova, E. Mikhailov, M. Fleischhauer, V.L. Velichansky, G.R. Welch, and M.O. Scully, Phys. Rev. A **62**, 023810 (2000).
[27] W. Happer, Rev. Mod. Phys. **44**, 169 (1972).
[28] F. Renzoni, S. Cartaleva, G. Alzetta, and E. Arimondo, Phys. Rev. A **63**, 065401 (2001).
[29] J.H. Xu and G. Alzetta, Phys. Lett. A **248**, 80 (1998); M. Graf, E. Arimondo, E.S. Fry, D.E. Nikonov, G.G. Padmabandu, M.O. Scully, and S.Y. Zhu, Phys. Rev. A **51**, 4030 (1995); E. Arimondo, *ibid.* **54**, 2216 (1996); S. Gozzini, P. Sartini, C. Gabbanini, A. Lucchesini, C. Marinelli, L. Moi, J.H. Xu, and G. Alzetta, Eur. Phys. J. D **6**, 127 (1999).